Trends in Satellite-Based Ocean Parameters through Integrated Time Series Decomposition and Spectral Analysis. Part II: NOAA/NCEI Blended Seawinds

KORAK SAHA,[a,b] PRASANJIT DASH,[c,d] JAMES FRECH,[a,b] HUAI-MIN ZHANG,[e] PAUL DIGIACOMO,[d] AND STEVEN D. MILLER[c]

[a] *Earth System Science Interdisciplinary Center, Cooperative Institute for Satellite Earth System Studies, University of Maryland, College Park, College Park, Maryland*
[b] *NOAA/National Centers for Environmental Information, Silver Spring, Maryland*
[c] *Cooperative Institute for Research in Atmosphere, Colorado State University, Fort Collins, Colorado*
[d] *Center for Satellite Applications and Research (STAR), NOAA/NESDIS, College Park, Maryland*
[e] *NOAA/National Centers for Environmental Information, Asheville, North Carolina*

(Manuscript received 20 January 2024, in final form 19 November 2024, accepted 9 January 2025)

ABSTRACT: Seawind is essential in studying extreme weather and climate events globally over the oceans. It has significant impacts through air–sea interactions, upper ocean mixing, and energy flux generation. The sea surface wind is also a critical element in blue economy strategic planning, offshore renewable energy, marine transportation, marine ecosystem, and fisheries. As per the Intergovernmental Panel on Climate Change (IPCC) working group report, there is low confidence level in wind trends due to insufficient evidence. This study uses signal decomposition, namely, the multiple seasonal-trend decomposition using locally estimated scatterplot smoothing (MSTL) on NCEI blended seawinds, version 2.0 (NBSv2.0; 1988–2022), to derive the nonlinear dynamic trend of global blended sea surface winds showing variations of 0.3–0.8 m s^{-1} and a global rate (linear approximation) of 0.022% ± 20% m s^{-1} $decade^{-1}$. Implementing MSTL requires specifying periods, which is achieved using time-dependent spectral wavelet analysis to extract significant seasonalities in the dataset. The calculated average trend rates are notably higher for the Southern Hemisphere oceans than for the Northern Hemisphere, with peaks ~0.1–0.15 m s^{-1} $decade^{-1}$ around the higher midlatitudes. Conversely, the tropical and near-equatorial bands show either a decreasing trend rate or weakly increasing trends. Areas with significantly increasing trend rates are mainly located in the west of the North Atlantic and the North Pacific, the Arctic, and the eastern tropical Pacific Ocean (ETPO)/central Pacific oceans, and a decreasing trend is visible over the rest of the Northern Hemisphere (specifically over the North Indian and the Northern Pacific oceans). In contrast, the Southern Hemisphere has mostly increasing trend rates except for the tropical southern Indian Ocean.

SIGNIFICANCE STATEMENT: Trends in global ocean winds are highly sensitive to the input data. Consequently, per the IPCC working group report, the trends reported over global winds are of low confidence. This study emphasizes that the trend of global neutral winds is a dynamic quantity that varies with time, and the globally reported trends (~0.08–1.2 m s^{-1} $decade^{-1}$) represent a linear approximation of this dynamic behavior. Most of these studies use an ordinary least squares fit to estimate this linear approximation. On the contrary, this analysis uses 35 years of high-quality and stable blended sea wind product developed from multiple satellites and estimates a more realistic long-term nonlinear trend by filtering out quasi-seasonal and high-frequency signals from the input data using a time series decomposition. This study leverages decomposition-based methods to reveal and quantify global sea wind trends, with a particular emphasis on understanding their variations across different latitude bands. This analysis provides global trend rate maps and explores the geospatial distributions of these trends. Our findings will assist in strategizing offshore wind energy development, understanding air–sea interactions, and disaster management.

KEYWORDS: Ocean; Sea/ocean surface; Satellite observations; Time series; Trends

1. Introduction

Among the various known essential climate variables (ECVs) over the ocean, the sea surface wind (SSW) is an important parameter that intrinsically affects the understanding of climate and its prediction. It is also essential for studying extreme weather events over the global ocean, such as tropical cyclones, extratropical storms, and high wind events (Seneviratne et al. 2012; Wang et al. 2023). Sea winds and wind stresses also significantly impact the air–sea interface, leading to changes in oceanic conditions through upper ocean mixing and energy flux (Donelan et al. 1997). Furthermore, SSW holds significant importance in the context of the blue economy strategic plan, the offshore renewable energy sector, marine transportation, marine ecosystems, fisheries, and other related domains. It is, therefore, of significance to understand the long-term trend of global ocean wind speeds to accurately forecast and apprehend the role of this ECV in climate change. According to a

Denotes content that is immediately available upon publication as open access.

Corresponding author: Korak Saha, korak.saha@noaa.gov

DOI: 10.1175/JTECH-D-24-0008.1

special report of working groups I and II of the Intergovernmental Panel on Climate Change (IPCC) (Seneviratne et al. 2012), confidence in wind trends is generally low due to insufficient evidence. Similarly, confidence in projections of changes in extreme winds remains low due to relatively few studies and existing shortcomings in these simulations, though there is medium confidence that the number of midlatitude cyclones will decrease in each hemisphere due to future anthropogenic climate change. Conversely, simulation studies using climate models indicate that the probability of intense tropical cyclones (TCs), on average, doubles globally in all the ocean basins except the Gulf of Mexico and the Bay of Bengal (Bloemendaal et al. 2022). There is limited confidence in the specific geographical projections of midlatitude cyclone activity and moderate confidence in the anticipated poleward displacement of midlatitude storm tracks owing to future anthropogenic influences (Seneviratne et al. 2012). These factors underscore the need for accurate, long-term trend analyses of wind data to address current knowledge gaps and enhance our understanding of global sea winds.

Several studies have focused on estimating trends in ocean surface wind speed, and their findings reveal a notable diversity in the reported values. For example, the derivative of trend (with time), hereafter referred to as trend rate, reported in terms of linear approximation using satellite-based radiometric data from 1987 to 2008 ranges between 0.08 and 0.084 m s^{-1} $decade^{-1}$ (~1.0% $decade^{-1}$) (Wentz et al. 2007; Tokinaga and Xie 2011; Zheng et al. 2022). Other recent studies (using satellite altimeter measurements and blended or reanalysis products) state these values in the range from 2.5% (0.187 m s^{-1} $decade^{-1}$) to 5% (0.375 m s^{-1} $decade^{-1}$) $decade^{-1}$ with a maximum reported value of ~1.2 m s^{-1} $decade^{-1}$ (Sterl and Caires 2005; Young et al. 2011a; Zheng et al. 2016). However, observations by Wentz and Ricciardulli (2011) regarding the work of Young et al. (2011a) assert that the latter's analysis, based on 23 years of satellite-derived altimetry data, overlooks the extended dataset of satellite-based microwave radiometer information. Furthermore, they proposed that a potential 2.5%–5% $decade^{-1}$ increase in wind speeds will lead to a consequential 5%–10% rise in evaporation and precipitation over two decades, considering a constant relative humidity. Given the implausibly substantial increase in precipitation, Wentz and Ricciardulli (2011) concluded that the trend approximations presented by Young et al. (2011a) are overstated. Young et al. (2011b) acknowledged the possibility of overestimating trends derived from altimeter data compared to radiometer-based data. However, the latter asserted that although this overestimation ranged between 1.4% and 2.4% $decade^{-1}$, the altimeter-based trends are consistent with buoy data but acknowledged that combined long-term data from altimeters, radiometers, and scatterometers would provide more reliable answers. More recently, results from Young and Ribal (2019) show that even though the spatial distributions of the radiometer and altimeter wind speed trend rates appear very similar (the radiometer being smoother, as expected due to their data abundance as compared to the altimeter), the radiometer trends are ~25% smaller than those of the altimeter and attributes this difference to the changes in boundary layer shape associated with atmospheric stability. Here, one should keep in mind the fact that altimeters estimate wind differently than scatterometers or radiometers. Altimeter-based wind products use the mean square slope of surface waves, rendering them sensitive to wave parameters (Li et al. 2013). On the other hand, scatterometers and radiometers measure the equivalent neutral (EN) wind, which is sensitive to wind stress and atmospheric stratification. This may also contribute to the unrealistic differences between the altimeter-based and scatterometer/radiometer-based trends.

The concept of a trend is commonly characterized as the "general direction and tendency" (Esterby 1993), and its estimation for any physical parameter, such as wind speeds, can diverge based on the methodology employed. Researchers have traditionally employed model fits like linear or Poisson regression or smoothing techniques like moving average, etc., to derive this trend. A trend has also been defined as the time series component representing the time variation of low-frequency mode (Organisation for Economic Co-Operation and Development 2007), and to identify the lower frequency modes, one has to eliminate the prevailing higher/medium frequency fluctuations. This can be achieved through signal decomposition, which is another method of trend estimation. Visser et al. (2015) provide a comprehensive read on definitions of trend, trend increment (rate), and several methods used to estimate the same. Following Chandler and Scott (2011), they broadly categorized trend methods into five classes which are exploratory, parametric, nonparametric, stochastic, and miscellaneous and provided a brief review on several trend models under these categories. It is essential to highlight that the trend values of wind speed mentioned in the preceding paragraph represent the average rate of change (derivative) observed over a specific time interval. However, it is the actual pattern of the time series of this low-frequency component that represents the trend in a physical parameter. Several nonparametric techniques commonly used for trend detection are recapitulated in the companion paper (Dash et al. 2025, hereafter Part I). The paper compares ordinary least squares (OLS) regression with three incrementally advancing decomposition methods: simple moving average (SMA), seasonal-trend decomposition using locally estimated scatterplot smoothing (LOESS) (STL), and multiple STL (MSTL). The concurrent implementation of several decomposition methods suggested that among the methods assessed, MSTL is most suited for estimating trends in long-term data as it enables multiple-period extraction.

This study employed MSTL to decompose long-term ocean surface blended sea winds described in section 2 to obtain the trend, multiple seasonal periods, and residual components. A time-dependent spectral analysis using wavelet transform is used to identify the dataset's major seasonalities (periods). MSTL then applies the STL algorithm iteratively to each of these periodic frequencies, and the trend time series is estimated using the last iteration. Like in any decomposition method, the residuals are also calculated by detrending and deseasoning the original signal. This study is performed both globally and over the zonal average, which is the average wind circulating at the same latitude band parallel to the

equator, averaging the atmosphere longitudinally. Our findings will assist in strategizing offshore wind energy development, understanding air–sea interactions, and disaster management. It will also be important to understand the projection of wind (windiness) and its effect on wave heights. In the following sections, we introduce the datasets used in this study, briefly introduce the trend estimation method, and discuss the results from our analysis.

2. Data

The U.S. National Oceanic and Atmospheric Administration (NOAA) National Centers for Environmental Information's (NCEI) Blended Seawinds (NBS) is an important product in considering NOAA's Blue Economy Strategic Plan, supporting mission areas in offshore renewable energy (wind farms), marine transportation, marine ecosystem, and fisheries. The latest version of this product (NBSv2.0) (Saha and Zhang 2022) was developed blending observations from multiple satellites including scatterometers and radiometers/imagers using a multisensor data fusion technique weighted by inherent errors of each product, to resolve very high winds associated with hurricanes and storms (Wang et al. 2023). Most of the dataset used in this blended product derive winds from a range of microwave observations including low and medium frequencies (~11–37 GHz) and very low-frequency (C-, L-, and X-band)-based radiometer winds. Winds speeds retrieved from platforms like SMAP (in L bands ~1.4 GHz) and a combination of C and X bands from AMSR2 reduce rain contamination and retrieve high wind speeds. Scatterometer winds derived from both C and Ku bands are also used in this product. Thus, NBSv2.0 is a global gap-free 10-m EN wind dataset that goes back to 1987 and is also generated in near–real time. The data are publicly accessible through the NOAA CoastWatch program (https://coastwatch.noaa.gov/cwn/products/noaa-ncei-blended-seawinds-nbs-v2.html) and are archived at NCEI. Being a well-calibrated, uninterrupted, long-term gap-free, and stable dataset [comparison of this product with other existing blended global products like CMEMS provides a long-term bias of ~0.03 and rsmd ~0–5 m s^{-1} (Saha and Zhang 2022), and the results are very similar when compared with in situ measurements] makes it an excellent candidate for investigating trends in global wind speeds. For this study, we used the daily mean wind speeds from NBSv2.0. In addition to daily data, 6-hourly and monthly mean periods are also available for interested users.

3. Trend estimation of global wind speed

Trends in datasets represent fundamental patterns that provide insights into the behavior of systems and phenomena. While the concept of a trend may seem self-evident, its rigorous definition and identification pose challenges that data analysts must address to extract meaningful information from data. By understanding the nuances of trends and employing appropriate analytical techniques, data analysts can leverage trend analysis to gain valuable knowledge and make informed decisions. The trend in scientific analysis encompasses a broad

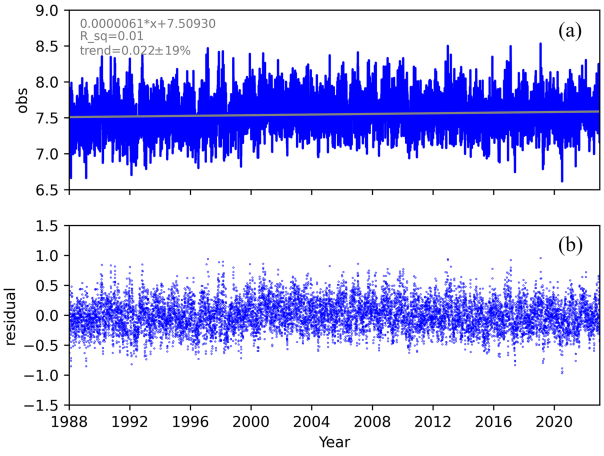

FIG. 1. (a) Global mean blended seawind time series with an OLS linear fit line (gray) and (b) the residual value representing the variability of the actual nonlinear data from an estimated linear approximation of trend.

spectrum of interpretations, each serving a distinct purpose. In some instances, a trend is perceived as an overarching tendency that permeates the entire data domain, extending into the realm of future observations. This perspective aligns with the notion of forecasting or predicting future behavior based on past patterns. Alternatively, a trend can be viewed as the anomaly component of a dataset after eliminating high-frequency fluctuations or noise. This approach emphasizes the underlying long-term behavior of the system, filtering out transient or short-lived variations. The choice of trend definition depends on the specific context of the analysis and the nature of the data.

In all the previously mentioned studies involving long-term ocean winds, the perspective of estimating an overall tendency for the dataset leads toward using a linear rate of change of trend estimation often misrepresented as the actual trends. Generally, this trend rate is quantified by estimating the slope using a simple linear regression based on OLS data fit (Kahane 2007). Figure 1a shows the time series of global mean sea surface wind speeds or observations (obs) obtained from NBSv2.0 and an OLS linear fit line (in gray). The slope of this line or trend rate and a margin of error (MOE) are also estimated from the observed data. The estimated value of the trend rate is ~0.022 m s^{-1} $decade^{-1}$, with a 19% margin of error (±0.004 m s^{-1}). The p value for this positive trend is <0.01, giving strong evidence in favor of the alternative hypothesis. It is clear that the linear least squares regression fit makes little sense of describing the actual trend (a dynamic quantity), which has interannual as well as seasonal variability. If one considers the anomaly/residual value representing the variability of the actual nonlinear data from an estimated linear approximation of trend (Fig. 1b), it clearly has a prevailing multidecadal time scale intact from the original data. Also, the lapse rate of the linear trend line could entirely flip the sign if the period of this analysis is changed or selectively chosen for a particular period. Another common

method that considers the trend as varying with time uses the decomposition-based smoothing technique and is a better representation of a changing trend in nonstationary and nonlinear data like ocean winds, and this is discussed further.

The LOESS is a locally weighted nonparametric regression for smoothing data in which no assumptions are made about the underlying structure of the data (Cleveland 1979). LOESS employs a local regression technique that combines elements of kernel regression and the running line smoother to fit a smooth curve through a scatterplot of data (Ryan 1997). It fits the data Y_i observed at the time t_i in each neighborhood using a weighted least squares fit, where the weights are developed from the distances of each t_i from t_0 (where predicted values are to be obtained). Using such local regression, a linear regression equation is determined for each segment (localized neighborhood), resulting in a model or trend, possibly in polynomial terms. Although robust estimates are generated using LOESS, the background assumption is that the errors can be specified to be either normally distributed or to have another symmetric distribution. Two LOESS-based methodologies are considered here.

a. STL

The STL is a nonparametric regression-based decomposition method for time series analysis (Cleveland et al. 1990). It uses a smoother tool for describing the trend in data as a function of one or more regressors. The smoothing in STL is performed using LOESS, which helps create a smooth line along the time plot to help see relationships between variables and foresee trends. STL is a versatile and robust method for decomposing time series into three components: trend, seasonal, and residual. If the data are represented as Y_v, trend, which is dynamic in nature (time varying), is represented as T_v with seasonal components as S_v and residual as R_v. The following expression can be established with v as the number of samples:

$$Y_v = T_v + S_v + R_v. \tag{1}$$

Using the STL decomposition on long-term ocean surface blended sea winds NBSv2.0, the signal is decomposed into a single seasonal component, and the trend is derived by LOESS regressor, and removing both the seasonal component and the trend from actual signal provides with the residual values. The time series data span from 1988 to 2022. Also, the missing days (very few, <1%) were imputed by linear interpolation, as STL will not work if the time series is not continuous. In this analysis, the global daily mean ocean surface wind is considered as the dependent variable (y axis of Fig. 2a) and the time as the independent variable (x axis of Fig. 2a). LOESS is used to smooth out the dependent variable (wind) as a function of time and compute a regression curve using a selective neighborhood weighting function (Cleveland et al. 1990) based on the proximity of the neighboring values. A polynomial of a certain degree is then used to fit the data using the weighting function. STL has a two-step process, the inner loop, which includes seasonal smoothing and detrending of the data, and the outer loop calculates the residuals by removing the seasonal and trend components from the data. Figure 2a shows the global mean wind data (obs), and the three components from Eq. (1), along with an OLS fit line (in gray) over the trend data, are shown in Figs. 2b and 2d. As STL decomposes the wind data time series into three components, trend, season, and residual, it uses the LOESS to extract smooth estimates of the three components. In this process, the three inputs used are the length of the seasonal smoother (season), the length of the trend smoother (trend), and the length of the low-pass estimation window (low pass), usually the smallest odd number larger than the periodicity of the data. The frequency of the wind data is also provided in terms of the periodicity of the data. The robust value was set to "True" to make a robust estimate, as it tolerates larger errors, visible in residuals in the lowermost panel of Fig. 2. To summarize, the trend and trend rate estimation have four major steps. In the first step, the process involves gap filling the missing data from the time series and determining dominating seasonal frequency, followed by step 2, where STL is used, iteratively, to extract the seasonal component and provide the nonlinear polynomial fit to data using LOESS (blue line in Fig. 2b), representing a dynamic trend. In step 3, the residuals (Fig. 2d) are estimated by subtracting the dynamic trend and seasonal component (Fig. 2c) from the original signal (Fig. 2a). The final step is estimating the linear trend rate (gray line in Fig. 2b), using linear fit to the dynamic trend (blue line). Compared to the residuals in OLS-based trend estimation (Fig. 1b), which contains a dominant multidecadal time scale, STL-based trend hardly has any noise (most of the residual values are closer to zero line–Fig. 2d).

The dynamic trend ranges between 7.43 and 7.65 m s^{-1}, and the trend rate values estimated from Fig. 2b are ~0.024 m s^{-1} $decade^{-1}$ with the margin of error of 18% (~0.0043 m s^{-1}). While implementing STL (information on packages for STL are detailed in data availability statement), a constant annual periodicity is used as a seasonal pattern; this can be disadvantageous for high-frequency data (such as hourly and daily data). Like any other real-world time series data, wind speed from NBSv2.0 can exhibit multiple seasonal patterns that are structurally unnested and interlacing together. Therefore, we used the computationally efficient MSTL (Bandara et al. 2021) procedure to minimize such seasonal mixing by incorporating STL implementation iteratively at multiseasonal frequencies.

b. MSTL

The MSTL is a fully automated extended version of STL decomposition that can handle multiple periodicities (Bandara et al. 2021), where an iterative approach is used to determine the multiple seasonal components in a time series. The advantage of MSTL decomposition is that it allows the separation of higher seasonal components from their corresponding lower ones. This also helps to make the trend smoother and devoid of any dominant seasonal components. Once the dominating seasonal components of the time series are determined, MSTL applies the STL algorithm iteratively to each of the identified seasonal frequencies and computes the dynamic trend using the last iteration of STL, which is further subtracted from the

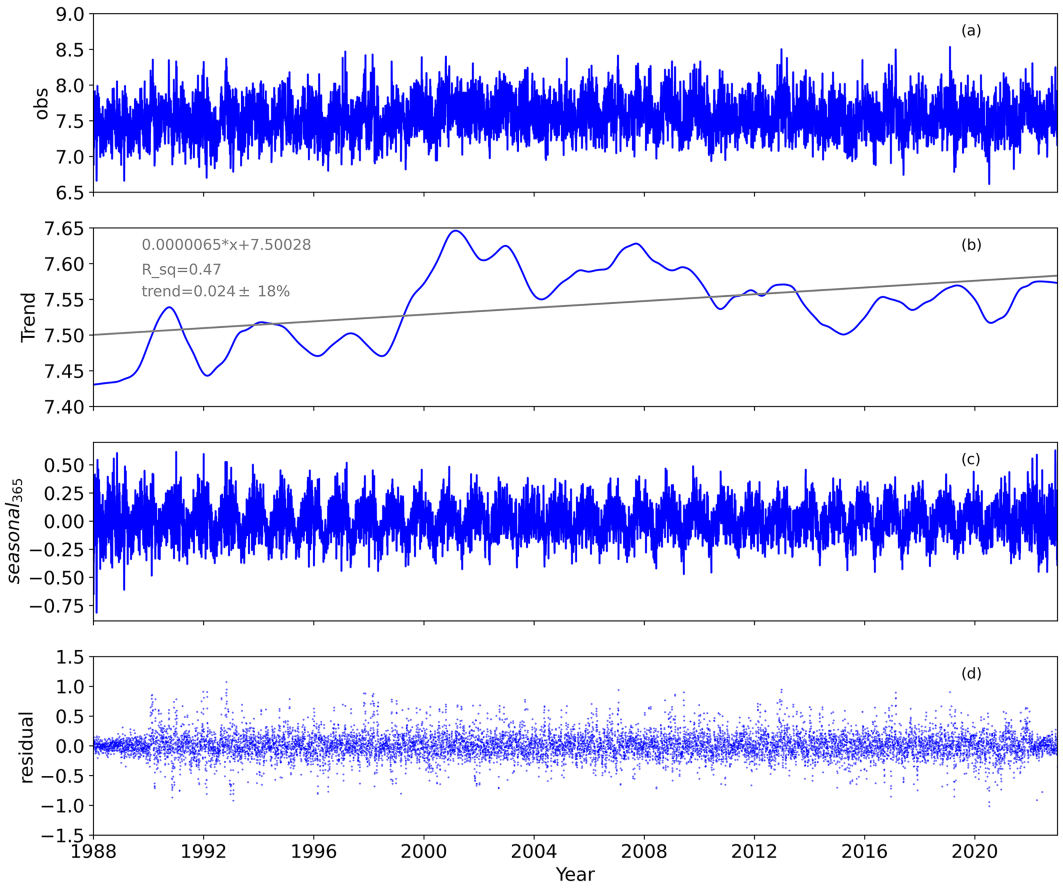

FIG. 2. (a) Global daily mean of NOAA NBSv2.0; (b) time variation of the trend value obtained applying the STL decomposition over the wind data; (c) this subplot shows the dominant seasonality (~annual periodicity) in this dataset; (d) the noise or residual component in the data.

seasonally adjusted time series to obtain the residual part. For data with no visible seasonality, MSTL uses Friedman's super smoother function (Friedman 1984) (https://github.com/jakevdp/supsmu/blob/master/README.md) to estimate the trend directly and further derive the residuals from the original time series. MSTL modifies Eq. (1) (from STL) to include multiple seasonal frequencies (S_v^1, S_v^2, ..., S_v^n) as follows:

$$Y_v = T_v + S_v^1 + S_v^2 + \cdots + S_v^n + R_v, \tag{2}$$

where n represents the numbers of the periods present in the time series Y_v. Following the algorithm provided by Bandara et al. (2021), the seasonal components, especially those smaller than half the series' length, are first determined and sorted in ascending order. The data are interpolated to avoid missing data, and STL decomposition for each seasonal cycle is implemented similar to what is mentioned in the previous subsection. Thus, the key inputs into MSTL other than the periodicities are the length of seasonal smoother with respect to each period (windows). Similar to step 1 in STL, it is very important to identify the relevant seasonal frequencies, which can be obtained from spectral analyses like principal component analysis (PCA), fast Fourier transformation (FFT), or wavelet analysis (Wavelet).

1) DERIVING DOMINATING SEASONAL FREQUENCIES USING WAVELETS

The wavelet transform and the windowed Fourier transform are both valuable tools for analyzing the frequency content of signals. However, they differ in their approach and suitability for different applications. The wavelet transform utilizes a series of wavelets, which are localized functions with varying scales, to decompose a signal into its constituent frequency components. This multiresolution analysis allows for the simultaneous examination of both time and frequency information. On the other hand, the windowed Fourier transform, also known as the short-time Fourier transform (STFT), divides a signal into segments and applies the Fourier transform to each segment. This method provides a localized view of the frequency content but lacks the temporal resolution of the wavelet transform. Both the methods help identify the predominant modes of variability in a time series of data. However, only the wavelet provides a continuous evolution of the frequency content over time. Therefore, in this analysis, to derive the dominating frequencies accurately and to

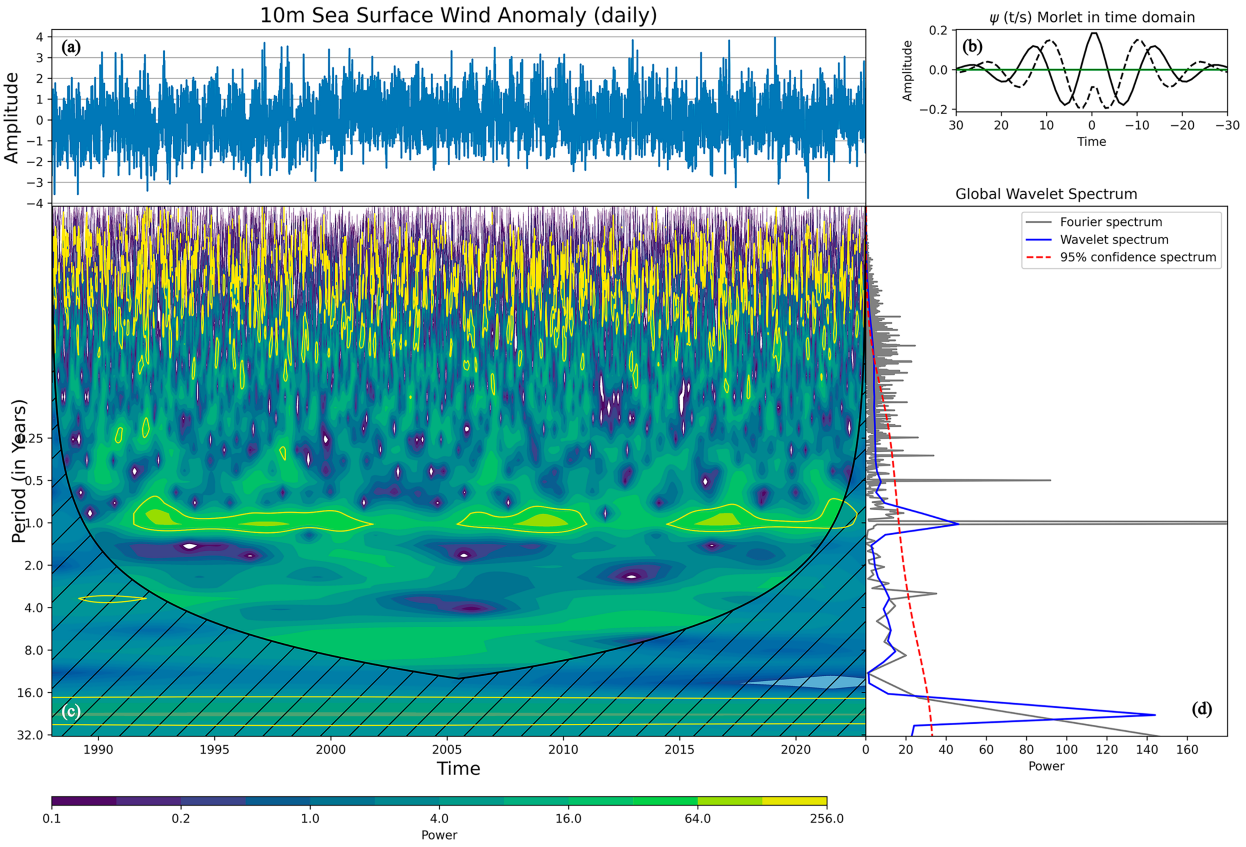

FIG. 3. (a) Time series of daily SSW anomaly (NBSv2—long-term global mean), which is subjected to wavelet analysis; (b) the wavelet function (Morlet) used in this analysis; (c) the normalized wavelet power spectrum, where thick yellow contours enclose regions of greater than 95% confidence with lag 1 autocorrelation coefficient of 0.84 and the mesh regions on either end indicate the "COI"; (d) the Fourier (gray) and wavelet (blue) spectrum peaks with 95% confidence spectrum in dashed line.

make sure they are consistently observed throughout the time period, we prefer a wavelet transform over a windowed Fourier transform. Torrence and Compo (1998) provide a detailed step-by-step wavelet analysis over El Niño–Southern Oscillation. In this paper, this work forms the basis for implementing the wavelet transform in wind speed data. A Python-based wavelet library, Waipy (https://github.com/mabelcalim/waipy), is used for this analysis and is implemented on the time series of the average deviation of daily global mean sea surface wind data from the long-term mean (or wind anomaly shown as amplitude in Fig. 3a), available for 35 years. As we use a continuous wavelet transform for this analysis, we must choose a wavelet function [$\psi_o(\eta)$], of a nondimensional time parameter, to analyze the time series and provide many different frequencies, each with nonstationary power (Daubechies 1990). In this analysis, we used the Morlet wavelet [Eq. (3) and Fig. 3b], which is a complex-valued function developed by modulating a Gaussian function (Schneider and Farge 2006):

$$\psi_o(\eta) = \pi^{-1/4} e^{(i\omega_o \eta)} e^{(-\eta^2/2)}, \tag{3}$$

where ω_o is a nondimensional frequency with a value of 6 to satisfy the admissibility condition (Torrence and Compo 1998). This complex form of Morlet wavelet results in a wavelet transform $W_n(S)$, which is also complex in nature [Eq. (4)]:

$$W_n(S) = \sum_{k=0}^{N-1} \hat{x}_k \hat{\psi} \times (S\omega_k) e^{i\omega_k n \delta t}, \tag{4}$$

where $W_n(S)$ being a complex variable has both real and imaginary parts represented by its amplitude and phase, with the wavelet power spectrum defined as the mod square of the wave transform term $|W_n(S)|^2$. Figure 3c shows the wavelet power spectrum normalized with the reciprocal of variance ($1/\sigma^2$), representing a measure of the power relative to the white noise. It is evident that the predominant power values are for the period of 1 year (~365 days), followed by a second prominent peak around 0.5 years (~183 days). The major peaks, along with numerous other peaks, are also observed in the Fourier spectrum (gray line) as well as the wavelet spectrum (blue line) in Fig. 3d. However, it should be noted here that the wavelet approximation spectrum and Fourier spectrum though equivalent are not necessarily identical in quantity; therefore, the 183 days peak is more prominent in later than the former, but a clear quasi-biennial oscillation for this 0.5-yr mode is also visible in the wavelet spectrum with

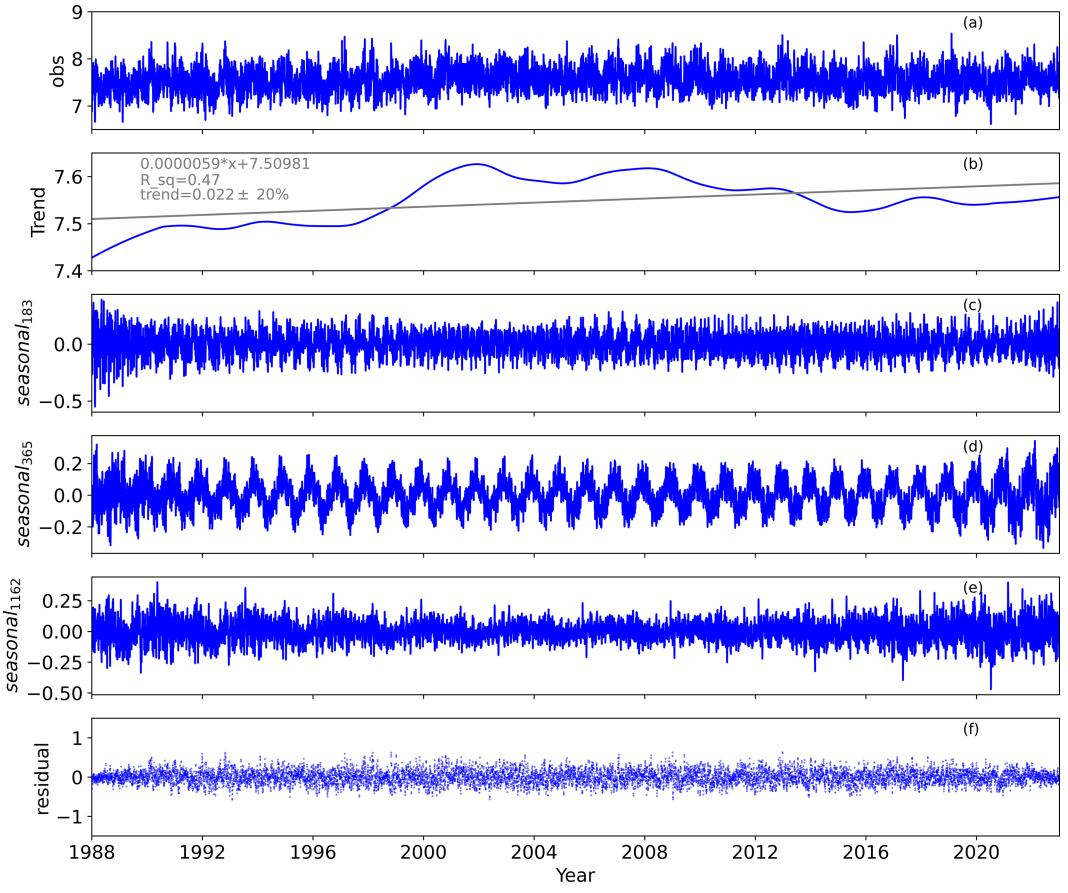

FIG. 4. As in Fig. 2, but multiple seasonality is implemented using the MSTL-based decomposition. (a) Time series of the global SSWs, (b) variation of the trend with time, (c)–(e) dominant seasonality (183, 365, 1162 days) components' time series, and (f) residual or the noise component.

reduced amplitude (Fig. 3c). The 95% confidence spectrum (or significance at a 5% level), which is a test for power being a true feature against the background power level in the signal, for the global seawinds is denoted by the dashed red curve in Fig. 3d and the area inside the yellow contour in Fig. 3c, for a lag 1 autocorrelation factor of 0.84. Such high correlation coefficient between tth value and $(t-1)$th value (lag 1 condition) shows that the data are serially correlated in time and are very stable. The cone of influence (COI) (represented by the mesh regions in Fig. 3c) is the region of the wavelet spectrum where the edge-effect artifacts play a role making the power coefficients unreliable (Torrence and Compo 1998) and thus is excluded from the analysis.

2) SPECIFYING SEASONAL FREQUENCIES IN MSTL

In our MSTL implementation using a Python package (https://www.statsmodels.org/), we used the abovementioned wavelet transform module to estimate the seasonal frequencies and used the multiple dominant frequencies (or seasonalities) as inputs for periods. Figure 4 shows the output when MSTL is applied to the daily global mean NBSv2 winds. Moving down from the top, each panel represents the original data (obs), the trend, and three prominent seasonalities (of 183, 365, and 1162 days), followed by the residuals. As described in the companion paper (Part I), MSTL provides a time-period variation of the trend which ranges from 7.42 to 7.6 m s^{-1} (Fig. 4). The linear approximation of the rate of change of this global ocean wind speed trend is also represented by the gray line in Fig. 4b. The trend rate shows a value of 0.022% ± 20% m s^{-1} $decade^{-1}$, i.e., globally, the wind is increasing with a rate of 0.022 m s^{-1} $decade^{-1}$ with a margin of error of 20% ($\sim\pm0.004$ m s^{-1}). It is noticeable from Figs. 2 and 4 that the nonlinear trend approximations are smoother when multiple levels of decomposition are applied instead of a single seasonal mode in STL, although the trend rates are comparable. The time series of residuals or anomaly that represents the variability with respect to the trends (Figs. 2d and 4f) demonstrates that this variability (or noise) is not really distinguishable from the white noise. As more seasonal frequency modes are added to the analysis (e.g., from STL to MSTL), this random noise becomes more stable and closer to the zero line.

To demonstrate the validity of the trend values derived from MSTL, we computed the confidence interval using the mean, standard deviation, and sample size of the data. A confidence interval is the range of values derived from the

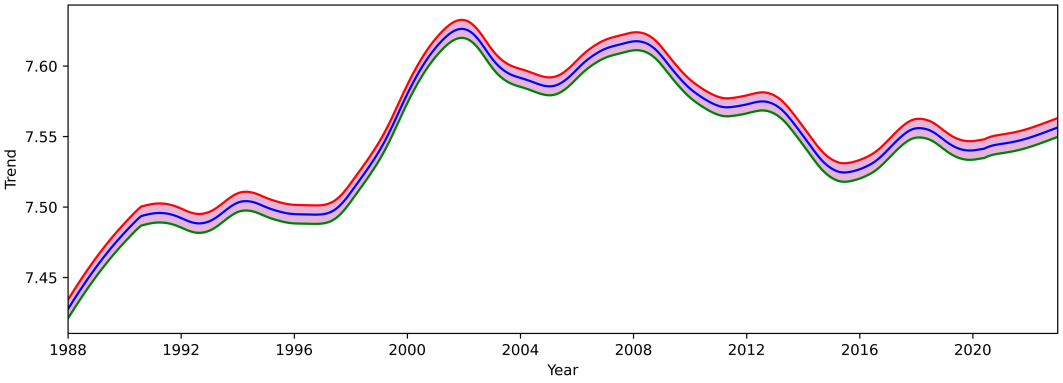

FIG. 5. Time series (m s^{-1}) of trend (blue) with the upper (red) and lower (green) bounds obtained by implementing a 95% confidence level.

statistics of a sample, which provides upper and lower bounds of the values between which the average mean of an ensemble exists. Here, we provide the 95% confidence interval (CI_{95}) using the following formula:

$$CI_{95} = \mu \pm Z\frac{\sigma}{\sqrt{n}}, \tag{5}$$

where μ is the mean value and σ is the standard deviation for a sample size of n. The z score calculated from the standard deviation Z is the interval between which the mean value exists. For a 95% confidence interval, the z score can also be obtained from the p value of linear regression (probability of the given statistical model when the null hypothesis is true) using a z-score table. From Eq. (5), with a z score of 1.96 (corresponding to the p value of 0.9750 and q value of 0.025) and mean and standard deviations obtained from the trend time series, an upper bound $[\mu + Z(\sigma/\sqrt{n})]$ and lower bound $[\mu - Z(\sigma/\sqrt{n})]$ of values are calculated as confidence intervals (Fig. 5). The upper bound is represented by a red line, and the lower bound is represented by green, with the actual trend in blue.

4. Zonal variation of wind speed trends

Near-surface wind speeds over the ocean facilitate interactions between the ocean and the atmosphere, serving as major drivers for ocean circulations and influencing fluxes associated with air–sea interactions (Zhai et al. 2012; Rodríguez et al. 2019). In the open oceans, the surface current affects the surface heat transfer, nutrients, and gases and modulates the atmospheric wind forcing (Rodríguez et al. 2019). The large-scale winds are also reported to drive rapid cross-basin transports of water masses, especially at low latitudes (Spall 2022). In the polar region, the winds and currents are responsible for the motion of sea ice and freshwater released from melting ice sheets (Rodríguez et al. 2019). In addition, the changing trend of ocean surface winds can affect coastal infrastructures and the offshore wind industry (Lyddon et al. 2019; Laurila et al. 2021). Therefore, a single global trend of surface wind speed is a simplified representation of the wind trends with both latitudinal and regional influences and is not valid for practical applications. In this analysis, we look into the zonal average of EN wind speed trends for every 10° latitudinal band between ±80°N and ±80°S (Figs. 6 and 7).

Figures 6a–h show the SSW trends and the trend rates (linear fits on the trend line) in gray for every 10° of the latitudinal band starting from 80°N to the equator. The trend time series shows that for every latitudinal band in the Northern Hemisphere, there is a notable trend variation that ranges between 0.3 and 0.8 m s^{-1} over the time period of 35 years. However, the rate of this trend is increasing (positive) from 80° to 40°N, and then, it switches to a decreasing (negative) rate between 40°N and the equator. These rates vary from 0.07 m s^{-1} $decade^{-1}$ in the high latitudes (>70°N), peaking at 0.1 m s^{-1} $decade^{-1}$ for the higher midlatitudes (between 50° and 70°N) and then falling to 0.03 m s^{-1} $decade^{-1}$ for lower midlatitudes. These rates become negative (decreasing rate) for the lower latitudes (20°N–0°) with −0.045 m s^{-1} $decade^{-1}$ for the extratropics (20°–30°N) and −0.07 m s^{-1} $decade^{-1}$ for the tropics (10°–20°N) with −0.01 m s^{-1} $decade^{-1}$ for the near-equatorial band (0°–10°N). The trend rates have similar behavior as we move toward the equator from 80°S (Figs. 7a–h), with negative rates starting from the 40°S and decreasing toward the equator and then peaking with 0.15 m s^{-1} $decade^{-1}$ at the higher midlatitudes (60°–50°S). Table 1 summarizes these values.

Similar observations of uneven distribution of trend rates are also reported in previous publications (Swart and Fyfe 2012; Zieger et al. 2014; Zheng et al. 2016, 2022), but a detailed zonal averaged study is attempted in this paper. The regional trends reported by both Young et al. (2011a) using altimetry data and Zheng et al. (2016) using the cross-calibrated, multiplatform (CCMP) wind data are approximately 1.5–2.5 times larger than the values reported here. Our results are realistically closer to the values reported by Wentz and Ricciardulli (2011), i.e., ~1.0% $decade^{-1}$, which also argues that a 2.5%–5% $decade^{-1}$ increase in winds [as reported by Young et al. (2011a)] would result in a 5%–10% increase in evaporation and precipitation in 20 years which is significantly higher than the reported values of global precipitation trends (Nguyen et al. 2018). However, it is worth noting that evaporation is a complex process dependent on multiple parameters, including wind speeds. The zonal trends of the wind speed from NBSv2.0 clearly show that the

FIG. 6. (a)–(h) Wind speed trends along with the rate of this trend (in gray) for every 10° of the NH latitudinal bands starting from 80°N to the 0° at the equator.

wind speeds are increasing at a higher rate over the mid- and high latitudes and are decreasing in values in the tropics and near equatorial regions. The wind trend rates over the equator are either insignificant or slightly decreasing.

5. Global map of trend rates in NBSv2.0 wind speeds

Winds over the oceans drive global ocean circulation, which can intensify surface warming, greater surface heat flux, and ocean heat content. These wind-driven ocean circulations can also lead to deeper mixed-layer depths, especially in the Southern Oceans (McMonigal et al. 2023). It is one of the crucial factors in the air–sea interactions and is closely related to the Southern Oscillation indices (SOIs) like El Niño and La Niña and other significant region-specific oscillations like North Atlantic Oscillations (NAOs) and Indian Ocean dipole (IOD) (Stopa and Cheung 2014). The long-term trends in parameters derived from wind speeds, e.g., wind power density, effective wind speed occurrence, and rich level occurrence of wind energy (or frequency of wind energy levels higher than 200 W m^{-2}), are important to plan the spatial distribution of offshore wind energy power plant sites and wind power utilization. Therefore, it is essential to study regional variabilities to understand the spatial variability of wind speed trends. To illustrate these regional differences, a map (Fig. 8a) of the trend rates is generated using 35 years for each 0.25° × 0.25° grid cell. Data used to generate this map are the monthly mean NBSv2.0 for the entire period. Therefore, we have 35 × 12 data points for each analysis grid cell in the time domain, with 719 × 1440 grid cells in the spatial domain. First, trends are calculated for each grid cell using MSTL, where the dominant periodicities are used to deseason the data and estimating the dynamic trend, followed by determining the trend rates using linear regression. It is noteworthy that the dominant periodicities are estimated individually at every grid point, which allows the method to account for the spatial variability of the data;

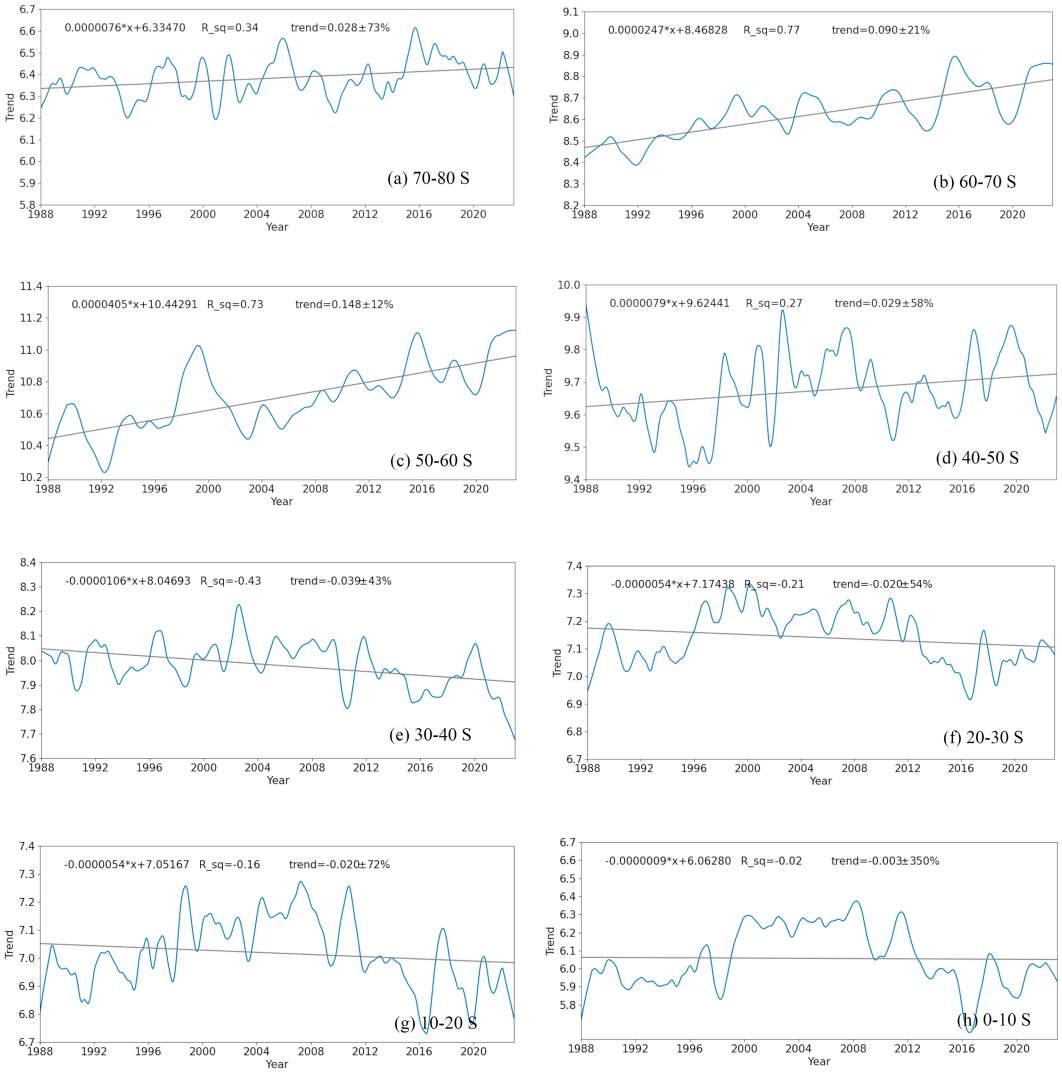

FIG. 7. (a)–(h) As in Fig. 6, but for SH latitudinal bands starting from 80°S to the 0° at equator.

however, it can be computationally expensive. The left panel of Fig. 8a also shows the latitudinal variation of longitudinally averaged trend rates, with red corresponding to averaged positive rates and blue being averaged negative rates. Figure 8b shows the probability density function corresponding to Fig. 8a.

There is a significant positive trend over the global oceans. Specifically, the positive values are higher over the Southern Hemisphere (SH). Increasing trend rates of ~0.2–0.45 m s^{-1} $decade^{-1}$ are observed over oceans in both the high midlatitude in the Southern Hemisphere (beyond 45°S) and the region beyond 60°N in the Northern Hemisphere (NH). These maximum values of trend rates are also visible in the zonal variation of average wind trends. However, some areas intermittently show negative trend rates from −0.1 to −0.3 m s^{-1} $decade^{-1}$ over these extremely high latitudes. Besides these regions, negative trends are also observed over the major NH ocean basins, such as North Pacific and North Atlantic, with values from −0.1 to −0.2 m s^{-1} $decade^{-1}$. These trend rates agree with the trends derived from multiple reanalysis data (Deng et al. 2021). In the NH oceans, the wind trends in the proximity of the equatorial region are predominantly negative, except for the eastern tropical Pacific Ocean (ETPO). The ETPO stretches along the Pacific coastline of Central America, spanning from southern Mexico to northern Peru. The trend is increasing over the ETPO and the central Pacific Ocean within the range of ~0.1–0.3 m s^{-1} $decade^{-1}$. This is an important region where the behavior of the wind and water are tightly intertwined during recurring El Niño and La Niña effects and can directly or indirectly affect weather patterns throughout the globe. These increasing values of trend rates over ETPO agree with a recent study by Yang et al. (2022) that reported a similar strengthening of Pacific trade winds since the mid-1990s, which could possibly be linked to the synergy of sea level pressure and sea surface temperature. The increase in wind speed trend rate over the North Atlantic is higher than in the North Pacific. However,

TABLE 1. The trend rates for every 10° zonal band between 80°N and 80°S with their corresponding MOE.

Lat	Trend rate (m s^{-1} $decade^{-1}$)	MOE (%)
70°–80°N	0.072	25
60°–70°N	0.082	36
50°–60°N	0.100	35
40°–50°N	0.030	105
30°–40°N	−0.01	238
20°–30°N	−0.045	30
10°–20°N	−0.07	18
0°–10°N	−0.011	81
0°–10°S	−0.003	350
10°–20°S	−0.02	72
20°–30°S	−0.02	54
30°–40°S	−0.04	43
40°–50°S	0.030	58
50°–60°S	0.150	12
60°–70°S	0.090	21
70°–80°S	0.027	75

in both these major ocean basins for higher northern latitudes (>~40°N), the western side has a higher positive trend than its eastern counterpart (e.g., trend rates over the western North Pacific Ocean are ~0.25 m s^{-1} $decade^{-1}$ as compared to ~0.05 m s^{-1} $decade^{-1}$ over the northeastern Pacific, and it is ~0.4 m s^{-1} $decade^{-1}$ in the western North Atlantic with lower values of ~0.1 m s^{-1} $decade^{-1}$ over its eastern side). Siemer et al. (2021), in their study over eastern North Atlantic Subtropical Gyre, along Northwest Africa and Western Iberia coast, clearly show an increasing trend in the meridional winds which is similar to the high value of wind speed trend rates observed over the same region in Fig. 8a. The Indian Ocean, encompassing approximately 29% of Earth's oceans (Wafar et al. 2011), is characterized by two significant intracontinental seas in its northern region, the Arabian Sea in the west, and the Bay of Bengal in the east. In the former, there is a notably weakened trend of around −0.01 m s^{-1} $decade^{-1}$, while the latter experiences a decreasing trend of approximately −0.2 m s^{-1} $decade^{-1}$. Over the Mediterranean waters, a strong increasing trend ranging between ~0.1 and 0.4 m s^{-1} $decade^{-1}$ exists. Yu (2021) also reports that over the last three decades, there has been an increasing trend (~0.2–0.4 m s^{-1} $decade^{-1}$) in winds over the Mediterranean, the Caspian, the Red, and the Black Seas but decreasing trend (up to ~0.3 m s^{-1} $decade^{-1}$) over the region dominated by the Asian summer monsoon (i.e., the Arabian, the Bay of Bengal, and the South China Sea). The trend in most of the southern Indian Ocean is decreasing at ~−0.15 m s^{-1} $decade^{-1}$. In the rest of the southern Indian

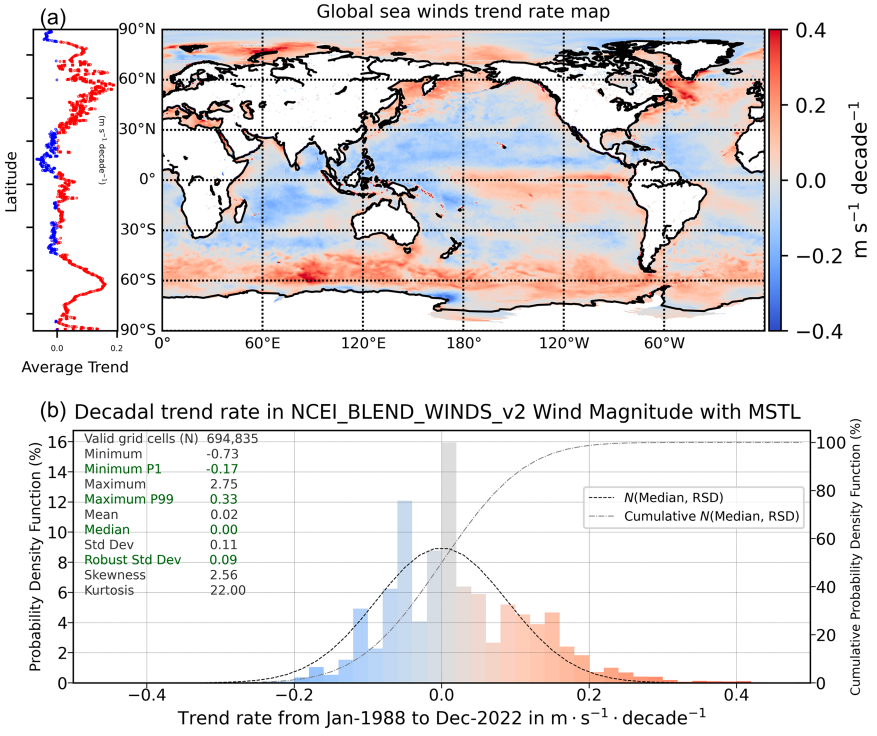

FIG. 8. (a) Global map of trend rates employing the MSTL 35 years of monthly mean wind data. The left plot shows the latitudinal variation of longitudinally averaged trend rates (with red for positive and blue for negative trend rates). (b) Decadal trend rate histogram for the values from (a) with color tables aligned. Statistical parameters are annotated to characterize the distributions: robust parameters are in green, while conventional ones are in gray. "Minimum P1" indicates the minimum value at the first percentile, and "Maximum P99" is the maximum at the 99th percentile. Normal and cumulative density functions are annotated in dashed lines.

Ocean, especially between 50° and 60°S, there is a very strong increasing trend <0.5 m s^{-1} $decade^{-1}$. Waugh et al. (2020) documented the trends in the Southern Hemisphere westerlies using the reanalysis winds at 850 hPa. Their results show an increase in the strength of zonal-mean winds in the Southern Oceans (beyond the 60°S) with a peak around the southern Pacific (trend of 0.3–0.45 m s^{-1} $decade^{-1}$), which is even larger than the Atlantic–Indian basin (reported to be between 0.1 and 0.2 m s^{-1} $decade^{-1}$) at those high latitudes. We see similar trends in EN winds at near sea level (10 m) with our analysis, where the peak is near the Atlantic–Indian basin (~0.1 m s^{-1} $decade^{-1}$) compared to ~0.3 m s^{-1} $decade^{-1}$ over the southern Pacific Ocean region. Overall, the spatial distribution of the wind speed trend rates ranges from −0.4 to 0.5 m s^{-1} $decade^{-1}$. However, this least squares–based rate of trend in each and every region can be strongly affected by its regional dynamics throughout the time period and may misrepresent the actual long-term trend.

6. Summary

This study used a decomposition-based approach to investigate long-term trends of ocean surface wind speeds. Specifically, the multiple seasonal-trend decomposition using LOESS (MSTL) method was implemented based on the moving least squares regression smoother. Wavelet analysis is used to decompose a time series of wind data into time–frequency space for determining the dominant modes of variability required as an input to MSTL. Using this information, the trend is obtained by polynomial smoothening of the data using LOESS regressor. The resulting trend is a time series in the same space as the original parameter, thus making it a dynamic quantity in place of a single curve-fitted parameter, often inaccurately referred to as the actual trend. The trend rate is the slope of the linear regression fit of the trend time series. Our value of the global trend rate estimated from 35 years of global surface sea winds is ~0.022% ± 20% m s^{-1} $decade^{-1}$, close to studies that used reanalysis and/or satellite radiometric data. These findings contrast with the trend rates derived from the altimeter-only data; however, we surmise that those trend rates are grossly overestimated. A trend analysis implemented over zonally averaged data shows that the wind trend rates have zonal variability, with higher values of ~0.09–0.1 m s^{-1} $decade^{-1}$ over the higher midlatitudes (with peaks around 50–60° in both hemispheres). The trend rates of seawinds are higher for the Southern Hemisphere than for the Northern Hemisphere. Tropical regions in both hemispheres show either a weakly increasing or decreasing trend. These rates decline for lower tropical latitudes with −0.04 m s^{-1} $decade^{-1}$ for the extratropics and −0.05 m s^{-1} $decade^{-1}$ for the tropics with −0.004 m s^{-1} $decade^{-1}$ for the near-equatorial band. The areas with significantly increasing trend rates are mainly located in the west of the North Atlantic and North Pacific Ocean basins, the Arctic Ocean, and the ETPO/central Pacific Ocean, and a decreasing trend is visible over the rest of the NH (specifically over the NIO and northern Pacific Ocean). Conversely, the SH has mostly increasing trend rates except for the tropical southern Indian Ocean. It must be emphasized here that although data used in this study are well calibrated, the trend and trend rate estimations are also affected by the uncertainty in the dataset, and further research is required in this context. As wind trend variability adds a valuable layer of foresight to wind energy projects, by choosing regions with sustained or increasing wind power potential, we can ensure the long-term viability of these investments and contribute to a more stable and predictable renewable energy landscape. Therefore, in future, it is intended to use the trend rate variability to identify regions with high wind energy potential, facilitating global offshore wind energy production.

Acknowledgments. This research is supported by NOAA/NESDIS National Centers for Environmental Information and Center for Satellite Applications and Research. NOAA Grants NA24NESX432C0001 and NA19NES4320002 (UMD CISESS) funded Korak Saha and James Frech and P. Dash was supported by NOAA Grants NA24OARX432C0007 and NA19OAR4320073.

Data availability statement. The multiple seasonal-trend decomposition using locally estimated scatterplot smoothing (MSTL) was implemented using the Stasmodel Python package [https://www.statsmodels.org/stable/generated/statsmodels.tsa.seasonal.MSTL.html#statsmodels.tsa.seasonal.MSTL; Bandara et al. (2021)]. STL was implemented using the python package [https://www.statsmodels.org/stable/generated/statsmodels.tsa.seasonal.STL.html#statsmodels.tsa.seasonal.STL; Cleveland et al. (1990), Seabold and Perktold (2010)]. The wavelet transform used a python-based package Waipy (https://github.com/mabelcalim/waipy). NOAA NCEI Blended Seawinds (NBSv2.0) data used in this study are publicly available from NOAA CoastWatch (https://coastwatch.noaa.gov/cwn/products/noaa-ncei-blended-seawinds-nbs-v2.html).

REFERENCES

Bandara, K., R. J. Hyndman, and C. Bergmeir, 2021: MSTL: A seasonal-trend decomposition algorithm for time series with multiple seasonal patterns. arXiv, 2107.13462v1, https://doi.org/10.48550/arXiv.2107.13462.

Bloemendaal, N., and Coauthors, 2022: A globally consistent local-scale assessment of future tropical cyclone risk. *Sci. Adv.*, **8**, eabm8438, https://doi.org/10.1126/sciadv.abm8438.

Chandler, R., and M. Scott, 2011: *Statistical Methods for Trend Detection and Analysis in the Environmental Sciences*. 1st ed. Wiley, 400 pp.

Cleveland, R. B., W. S. Cleveland, J. E. Mcrae, and I. Terpenning, 1990: STL: A seasonal-trend decomposition procedure based on loess. *J. Off. Stat.*, **6**, 3–33.

Cleveland, W. S., 1979: Robust locally weighted regression and smoothing scatterplots. *J. Amer. Stat. Assoc.*, **74**, 829–836, https://doi.org/10.1080/01621459.1979.10481038.

Dash, P., K. Saha, P. Digiacomo, S. D. Miller, H.-M. Zhang, R. Lazzaro, and S. Son, 2025: Trends in satellite-based ocean parameters through integrated time series decomposition and spectral analysis. Part I: Chlorophyll, sea surface temperature, and sea level anomaly. *J. Atmos. Oceanic Technol.*, **42**, 91–123, https://doi.org/10.1175/JTECH-D-24-0007.1.

Daubechies, I., 1990: The wavelet transform, time-frequency localization and signal analysis. *IEEE Trans. Inf. Theory*, **36**, 961–1005, https://doi.org/10.1109/18.57199.

Deng, K., C. Azorin-Molina, L. Minola, G. Zhang, and D. Chen, 2021: Global near-surface wind speed changes over the last decades revealed by reanalyses and CMIP6 model simulations. *J. Climate*, **34**, 2219–2234, https://doi.org/10.1175/JCLI-D-20-0310.1.

Donelan, M. A., W. M. Drennan, and K. B. Katsaros, 1997: The air–sea momentum flux in conditions of wind sea and swell. *J. Phys. Oceanogr.*, **27**, 2087–2099, https://doi.org/10.1175/1520-0485(1997)027<2087:TASMFI>2.0.CO;2.

Esterby, S. R., 1993: Trend analysis methods for environmental data. *Environmetrics*, **4**, 459–481, https://doi.org/10.1002/env.3170040407.

Friedman, J. H., 1984: A variable span smoother. Dept. of Statistics, Stanford University Tech. Rep. LCS5, 32 pp.

Kahane, L. H., 2007: *Regression Basics*. 2nd ed. Sage Publications, 240 pp.

Laurila, T. K., V. A. Sinclair, and H. Gregow, 2021: Climatology, variability, and trends in near-surface wind speeds over the North Atlantic and Europe during 1979–2018 based on ERA5. *Int. J. Climatol.*, **41**, 2253–2278, https://doi.org/10.1002/joc.6957.

Li, S., D. Zhao, L. Zhou, and B. Liu, 2013: Dependence of mean square slope on wave state and its application in altimeter wind speed retrieval. *Int. J. Remote Sens.*, **34**, 264–275, https://doi.org/10.1080/01431161.2012.713144.

Lyddon, C. E., J. M. Brown, N. Leonardi, and A. J. Plater, 2019: Increased coastal wave hazard generated by differential wind and wave direction in hyper-tidal estuaries. *Estuarine Coastal Shelf Sci.*, **220**, 131–141, https://doi.org/10.1016/j.ecss.2019.02.042.

McMonigal, K., S. Larson, S. Hu, and R. Kramer, 2023: Historical changes in wind-driven ocean circulation can accelerate global warming. *Geophys. Res. Lett.*, **50**, e2023GL102846, https://doi.org/10.1029/2023GL102846.

Nguyen, P., A. Thorstensen, S. Sorooshian, K. Hsu, A. Aghakouchak, H. Ashouri, H. Tran, and D. Braithwaite, 2018: Global precipitation trends across spatial scales using satellite observations. *Bull. Amer. Meteor. Soc.*, **99**, 689–697, https://doi.org/10.1175/BAMS-D-17-0065.1.

Organisation for Economic Co-Operation and Development, 2007: *Data and Metadata Reporting and Presentation Handbook*. OECD Publishing, 158 pp.

Rodriguez, E., M. Bourassa, D. Chelton, J. T. Farrar, D. Long, D. Perkovic-Martin, and R. Samelson, 2019: The winds and currents mission concept. *Front. Mar. Sci.*, **6**, 438, https://doi.org/10.3389/fmars.2019.00438.

Ryan, T. P., 1997: *Modern Regression Methods*. John Wiley and Sons, 515 pp.

Saha, K., and H.-M. Zhang, 2022: Hurricane and typhoon storm wind resolving NOAA NCEI Blended Sea surface wind (NBS) product. *Front. Mar. Sci.*, **9**, 935549, https://doi.org/10.3389/fmars.2022.935549.

Schneider, K., and M. Farge, 2006: Wavelets: Mathematical theory. *Encyclopedia of Mathematical Physics*, Elsevier, 426–438.

Seabold, S., and J. Perktold, 2010: Statsmodels: Econometric and Statistical Modeling with Python. *Proc. Ninth Python in Science Conf.*, Austin, TX, Enthought, Inc., 92–96, https://doi.org/10.25080/Majora-92bf1922-011.

Seneviratne, S. I., and Coauthors, 2012: Changes in climate extremes and their impacts on the natural physical environment. *Managing the Risks of Extreme Events and Disasters to Advance Climate Change Adaptation*, C. B. Field et al., Eds., Cambridge University Press, 109–230.

Siemer, J. P., and Coauthors, 2021: Recent trends in SST, chl-*a*, productivity and wind stress in upwelling and open ocean areas in the upper Eastern North Atlantic subtropical gyre. *J. Geophys. Res. Oceans*, **126**, e2021JC017268, https://doi.org/10.1029/2021JC017268.

Spall, M. A., 2022: Wind-forced variability of the zonal overturning circulation. *J. Phys. Oceanogr.*, **52**, 965–979, https://doi.org/10.1175/JPO-D-21-0174.1.

Sterl, A., and S. Caires, 2005: Climatology, variability and extrema of ocean waves: The Web-based KNMI/ERA-40 wave atlas. *Int. J. Climatol.*, **25**, 963–977, https://doi.org/10.1002/joc.1175.

Stopa, J. E., and K. F. Cheung, 2014: Periodicity and patterns of ocean wind and wave climate. *J. Geophys. Res. Oceans*, **119**, 5563–5584, https://doi.org/10.1002/2013JC009729.

Swart, N. C., and J. C. Fyfe, 2012: Observed and simulated changes in the Southern Hemisphere surface westerly wind-stress. *Geophys. Res. Lett.*, **39**, L16711, https://doi.org/10.1029/2012GL052810.

Tokinaga, H., and S.-P. Xie, 2011: Wave- and Anemometer-based Sea surface Wind (WASWind) for climate change analysis. *J. Climate*, **24**, 267–285, https://doi.org/10.1175/2010JCLI3789.1.

Torrence, C., and G. P. Compo, 1998: A practical guide to wavelet analysis. *Bull. Amer. Meteor. Soc.*, **79**, 61–78, https://doi.org/10.1175/1520-0477(1998)079<0061:APGTWA>2.0.CO;2.

Visser, H., S. Dangendorf, and A. C. Peterson, 2015: A review of trend models applied to sea level data with reference to the "acceleration-deceleration debate". *J. Geophys. Res. Oceans*, **120**, 3873–3895, https://doi.org/10.1002/2015JC010716.

Wafar, M., K. Venkataraman, B. Ingole, S. Ajmal Khan, and P. Lokabharathi, 2011: State of knowledge of coastal and marine biodiversity of Indian Ocean countries. *PLOS ONE*, **6**, e14613, https://doi.org/10.1371/journal.pone.0014613.

Wang, Z., K. Saha, E. S. Nyadjro, Y. Zhang, B. Huang, and J. Reagan, 2023: Oceanic responses to the winter storm outbreak of February 2021 in the Gulf of Mexico from in situ and satellite observations. *Remote Sens.*, **15**, 2967, https://doi.org/10.3390/rs15122967.

Waugh, D. W., A. Banerjee, J. C. Fyfe, and L. M. Polvani, 2020: Contrasting recent trends in Southern Hemisphere westerlies across different ocean basins. *Geophys. Res. Lett.*, **47**, e2020GL088890, https://doi.org/10.1029/2020GL088890.

Wentz, F. J., and L. Ricciardulli, 2011: Comment on "global trends in wind speed and wave height". *Science*, **334**, 905, https://doi.org/10.1126/science.1210317.

——, ——, K. Hilburn, and C. Mears, 2007: How much more rain will global warming bring? *Science*, **317**, 233–235, https://doi.org/10.1126/science.1140746.

Yang, F., L. Zhang, and M. Long, 2022: Intensification of Pacific trade wind and related changes in the relationship between sea surface temperature and sea level pressure. *Geophys. Res. Lett.*, **49**, e2022GL098052, https://doi.org/10.1029/2022GL098052.

Young, I. R., and A. Ribal, 2019: Multiplatform evaluation of global trends in wind speed and wave height. *Science*, **364**, 548–552, https://doi.org/10.1126/science.aav9527.

——, S. Zieger, and A. V. Babanin, 2011a: Global trends in wind speed and wave height. *Science*, **332**, 451–455, https://doi.org/10.1126/science.1197219.

——, A. V. Babanin, and S. Zieger, 2011b: Response to comment on "Global trends in wind speed and wave height". *Science*, **334**, 905, https://doi.org/10.1126/science.1210548.

Yu, L., 2021: Emerging pattern of wind change over the Eurasian marginal seas revealed by three decades of satellite ocean-surface

wind observations. *Remote Sens.*, **13**, 1707, https://doi.org/10.3390/rs13091707.

Zhai, X., H. L. Johnson, D. P. Marshall, and C. Wunsch, 2012: On the wind power input to the ocean general circulation. *J. Phys. Oceanogr.*, **42**, 1357–1365, https://doi.org/10.1175/JPO-D-12-09.1.

Zheng, C. W., J. Pan, and C. Y. Li, 2016: Global oceanic wind speed trends. *Ocean Coastal Manage.*, **129**, 15–24, https://doi.org/10.1016/j.ocecoaman.2016.05.001.

Zheng, C.-w., and Coauthors, 2022: Global trends in oceanic wind speed, wind-sea, swell, and mixed wave heights. *Appl. Energy*, **321**, 119327, https://doi.org/10.1016/j.apenergy.2022.119327.

Zieger, S., A. V. Babanin, and I. R. Young, 2014: Changes in ocean surface wind with a focus on trends in regional and monthly mean values. *Deep-Sea Res. I*, **86**, 56–67, https://doi.org/10.1016/j.dsr.2014.01.004.